

Variabilities of the spring river runoff system in East China and their relations to precipitation and sea surface temperature

Wen Chen,^{a*} Lin Wang,^a Yongkang Xue^b and Shufen Sun^c

^a Center for Monsoon System Research, Institute of Atmospheric Physics, Chinese Academy of Sciences, P.O. Box 2718, Beijing 100190, China

^b Department of Geography, Department of Atmospheric and Oceanic Sciences, University of California, Los Angeles, California 90095, USA

^c Institute of Atmospheric Physics, Chinese Academy of Sciences, Beijing 100190, China

ABSTRACT: The annual cycle and variabilities of the spring river runoff in East China (EC) at the continental scale and their relationship with precipitation, sea surface temperature (SST), and El Niño–Southern Oscillation (ENSO) are investigated. Monthly mean data from 72 runoff stations and 160 precipitation stations in EC, covering a period between 1951 and 1983, are used for this study. The seasonal evolution of runoff depth is generally consistent with that of the rainfall but has more regional characteristics. The dominant spatial patterns and temporal variations of spring runoff and precipitation are studied with the empirical orthogonal function (EOF) analysis. The leading EOFs of spring runoff and precipitation show the intensity of runoff and precipitation in South China and are highly correlated with each other, indicating a direct response of runoff to precipitation, which is different from the summer situation. Statistic analysis suggests that the evolution of ENSO event may exert a strong influence on these two modes. The second EOFs of runoff and precipitation present a north–south oscillation in EC with Nanling Mountain as the boundary and are also well correlated. These modes are highly related to the distribution of topography and may not be influenced by the ENSO. The third EOFs exhibit east–west oscillations in EC in both runoff and precipitation. The interdecadal relationship between spring precipitation/runoff and SST is further studied by singular value decomposition (SVD) analysis. The results indicate that the first coupled mode is dominant with the associated SST anomalies as an ENSO-like interdecadal SST signal and indicates pronounced warming (SST) and wetting (runoff) trends in North China after the mid-1970s, consistent with the observed trends of SST and runoff. The second coupled mode links the subtropical SST to the main spring runoff EOF mode in South China. Copyright © 2008 Royal Meteorological Society

KEY WORDS river runoff; precipitation; sea surface temperature

Received 13 April 2008; Revised 24 September 2008; Accepted 24 September 2008

1. Introduction

The Asian monsoon is one of the most energetic components of the Earth's climate system. Located in a strong monsoon region, East Asia has aperiodic and large-amplitude climate variability (e.g. Huang *et al.*, 2003). This variability and the influence from the coupled atmosphere–ocean system have been the subject of numerous studies (e.g. Huang and Sun, 1992, 1994; Zhang *et al.*, 1996; Lau and Weng, 2001). Continental-scale land–surface hydrological processes are essential components in monsoon dynamics. However, much less effort has been devoted to study the climate variability of ground macrohydrology for the East Asian region, partly due to lack of availability of data. Recently, large-scale hydrological processes are attracting more and more interest from the global climate research community as more

observational data are available (e.g. Lins, 1985; Lettenmaier *et al.*, 1994; Dirmeyer *et al.*, 1999; Fekete *et al.*, 2002; Maurer *et al.*, 2002; Li *et al.*, 2005). As one of the most important hydrological processes, runoff forms a large portion of the ground hydrology cycle. Studies of the large-scale hydro-meteorological processes are particularly relevant to Asian monsoon studies. Fewer analyses have been conducted for continental-scale river runoff, due to the difficulty in data collection and the uniqueness of river runoff data (Xue *et al.*, 2005).

In the Asian monsoon region, a major portion of water resources is provided by the summer monsoon (Lau *et al.*, 1988). Floods and droughts caused by the variability of the Asian summer monsoon are among the most devastating natural disasters, which impact a large segment of the world population. The East Asian monsoon floods and droughts are extremely variable in space and time. Often, the amplitude of the interannual variability can be as large as the mean state. Many studies (e.g. Lau, 1992; Yatagai and Yasunari, 1994; Nitta and Hu, 1996; Weng *et al.*, 1999) have shown

* Correspondence to: Wen Chen, Center for Monsoon System Research, Institute of Atmospheric Physics, Chinese Academy of Sciences, P.O. Box 2718, Beijing 100190, China. E-mail: cw@post.iap.ac.cn

that the observed precipitation exhibits strong interannual and interdecadal variations, as well as a long-term dry trend in East Asia. Meanwhile, different climate anomaly signatures appear over different parts of China (e.g. Xue, 1996), in particular, a dramatic shift from dry to wet conditions in the central eastern China and an opposite shift in the northern China in the late 1970s (Weng *et al.*, 1999).

A recent work of Xue *et al.* (2005) has investigated the spatial and temporal characteristics of East China's (EC) river runoff and their relationship with precipitation and sea surface temperature (SST) with data from 72 runoff stations for the period 1951–1983. Their study mainly documented the runoff variability in the summer and indicated a significant relation to the El Niño–Southern Oscillation (ENSO). However, the influence of ENSO on the East Asian water cycle, such as the rainfall, is not limited to summer (Zhang *et al.*, 1999; Wang *et al.*, 2000; Wu *et al.*, 2003). Furthermore, spring runoff and rainfall in some regions account for a considerable fraction of the total annual amount (see Section 3 for detail), thus making the spring variability important. Particularly, in southern China, the rainfall and its variability in spring is as large as that in summer. Therefore, understanding the interannual variations of the spring water cycle in East Asia and the influence from ENSO is as important as understanding those in the summer season.

This study investigates the interannual runoff variability, mainly during spring, in China at the continental scale and its relationship with precipitation, SST, and ENSO. The data sets and analysis methods applied in this study are introduced in Section 2, which is followed by a description of the basic climatology of runoff and precipitation in Section 3. In Section 4, we investigate the seasonal to interannual variations of spring precipitation and runoff in China and their covariability at continental scales. Section 5 discusses the relationship between precipitation/runoff and SST on both interannual and interdecadal timescales. Finally, a summary is presented in Section 6.

2. Data and analysis tools

For this study, we used the monthly mean river runoff data from 72 stations in China, as described in Xue *et al.* (2005). This dataset covers the period from 1951–1983 and was interpolated to 1° grid boxes based on the Total Runoff Integrating Pathways [TRIP, see Oki and Sud (1998) and Xue *et al.* (2005) for detailed descriptions]. The interpolated data have been proved to represent the seasonal mean condition well and compare well with published Chinese atlases (Xue *et al.*, 2005). We also employed the monthly mean precipitation data from 160 China stations obtained from the China Meteorological Administration (Chen *et al.*, 1998). This dataset spans from 1951 through 1999 and was also interpolated to 1° grid boxes using the Grid Analysis and Display System (GrADS) software. In addition, the monthly mean SST

data from the United Kingdom Hadley Centre (Parker *et al.*, 1999) with 1° horizontal resolution are used to check their relations to the runoff/precipitation. In this study, we focus only on the areas to the east of 105°E longitude because of the runoff data coverage. This region is referred to as EC and our discussions are restricted to within this region. The spring season covers the average of March, April and May (MAM). Please note that these two datasets were measured and recorded by two independent organizations: one is a hydrological network and the other is a meteorological network.

Empirical orthogonal function (EOF) analysis (North *et al.*, 1982; North, 1984; Storch and Zwiers, 1999) is used to obtain the dominant interannual modes of runoff/precipitation. This method allows for the individual extraction of the main patterns of each variable. The EOFs are orthogonal spatial patterns that can be thought of as empirically derived basic functions. The low-order EOFs can sometimes be interpreted as natural modes of variation of the observed system. The time coefficients that are obtained by projecting the observed field onto the EOFs, called *principal components* (PCs), are uncorrelated and represent the temporal variability of the field. In addition, a singular value decomposition (SVD) analysis (Bretherton *et al.*, 1992; Wallace *et al.*, 1992), which allows focus on the common patterns between two variables, is conducted to find the modes of covariability between the runoff/rainfall anomaly and the SST anomaly.

This article contains a number of names of Chinese rivers, mountains and lakes. These names are illustrated in a schematic map (Figure 1) together with the realistic topography in the EC.

3. Basic monthly mean climatology

Figure 2 presents the long-term mean annual cycle of precipitation/runoff depth averaged from 1951 through 1983 over the EC. The maximum monthly precipitation exceeds 160 mm/month, occurring in June, and the minimum is less than 25 mm/month, occurring in December. The average rainfall over the EC increases steadily from January to June at about 29.1 mm/month and drops from July to December at similar rate (28.8 mm/month). The evolution of runoff generally follows that of the rainfall, with the maximum (about 75 mm/month) in June and the minimum (less than 13 mm/month) in January. In contrast to the quasi-symmetric change rate of rainfall, the average rate of runoff depth increase in the first half year (13.5 mm/month) is higher than the decreased rate in the second half year (10.3 mm/month), possibly due to the melting of snow and ice. Previous studies (e.g. Chen *et al.*, 1998; Xue *et al.*, 2005) have pointed out that China's rainfall and runoff have obvious regional characteristics. Therefore, we will present the variations of regional distribution as well as the evolution of total amount.

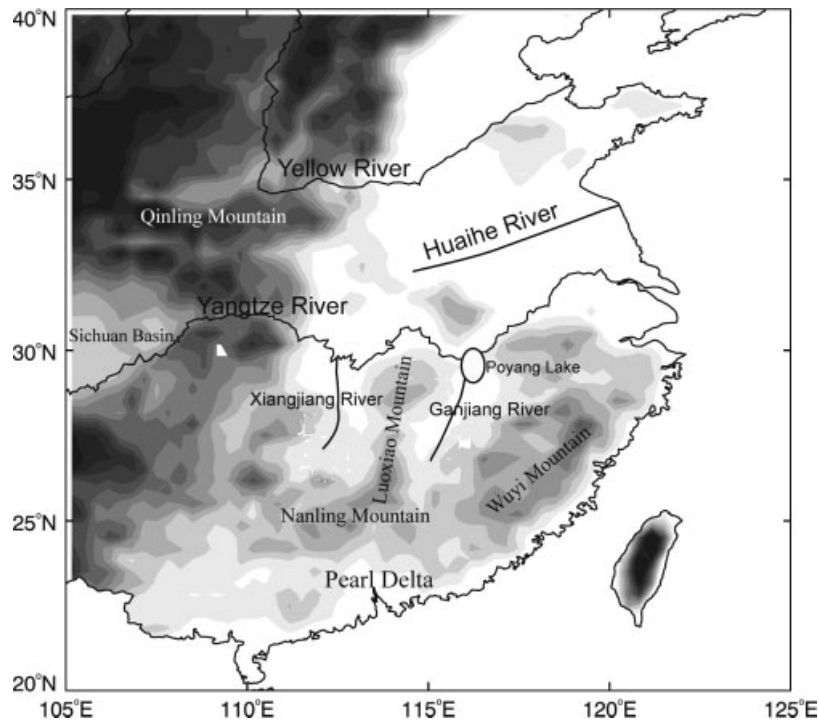


Figure 1. The schematic map of realistic topography in EC and the location of rivers, mountains and lakes mentioned in this article. The light to dark shading indicates the altitude from 150 to over 1800 meters.

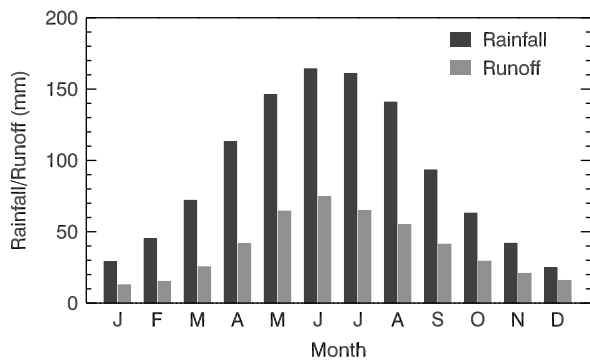


Figure 2. The long-term mean annual cycle of precipitation/runoff depth averaged from 1951 through 1983 over EC. Unit: mm/month.

Figure 3 illustrates the climatology of monthly mean precipitation/runoff depth distribution in the EC averaged from 1951 through 1983. The intensity of precipitation has great month-to-month variation with distinct southwest–northeast oriented belt-like distribution, which moves in the north–south direction with time (Figure 3(a)). In three winter months (December, January, and February), the precipitation is mainly confined to the areas south of 35°N with the maximum located north of the Nanling Mountain (around 24–26°N and 111–114°E) and east of the Poyang Lake (around 29°N and 117°E). In winter, the EC circulation of air is controlled by the northerly originating from the cold Siberian high system, and the monthly mean rainfall is less than 40 mm/month over most regions except to the south of the Yangtze River, where the rainfall stems mainly from the lifting of warm, moist southerly air by the cold

northerly flows. From March to May, the main precipitation belt is still located to the south of the Yangtze River, but the maximum increases rapidly from about 150 mm/month in March to over 300 mm/month in May, which corresponds to the pre-summer rainy season in South China resulting from the first step of East Asian summer monsoon (EASM) progress (Ding, 2004). Meanwhile, the precipitation in North China increases gradually to about 20–30 mm/month. From June to August, the main rain belt jumps rapidly from the Yangtze River Valley to the Yellow River Valley, and the precipitation generally exceeds 100 mm/month in most regions of the EC. In September when the EASM withdraws southward and out of China’s mainland (Ding, 2004), the precipitation drops below 100 mm/month over most of the EC except for the southeast coasts, where typhoon rainfall maximizes for the year, and north of the Sichuan Basin, where the topography and typhoons both account for continued precipitation (Zhuo *et al.*, 2000). With less and weaker moist southerly flow in October and November, the precipitation belt weakens and moves gradually to the south of the Yangtze River again. Clearly, the north–south movement of the rain belt is one of the most important characteristics of precipitation in the EC and leads to diverse peak times across the region.

The monthly variations of the runoff depth distribution (Figure 3(b)) by and large follow the monthly changes in precipitation distribution (Figure 3(a)) and directly respond to the rainfall of the same month from January to July. In these seven months, the spatial pattern of runoff depth compares well with those of precipitation, with the peak area mainly located between

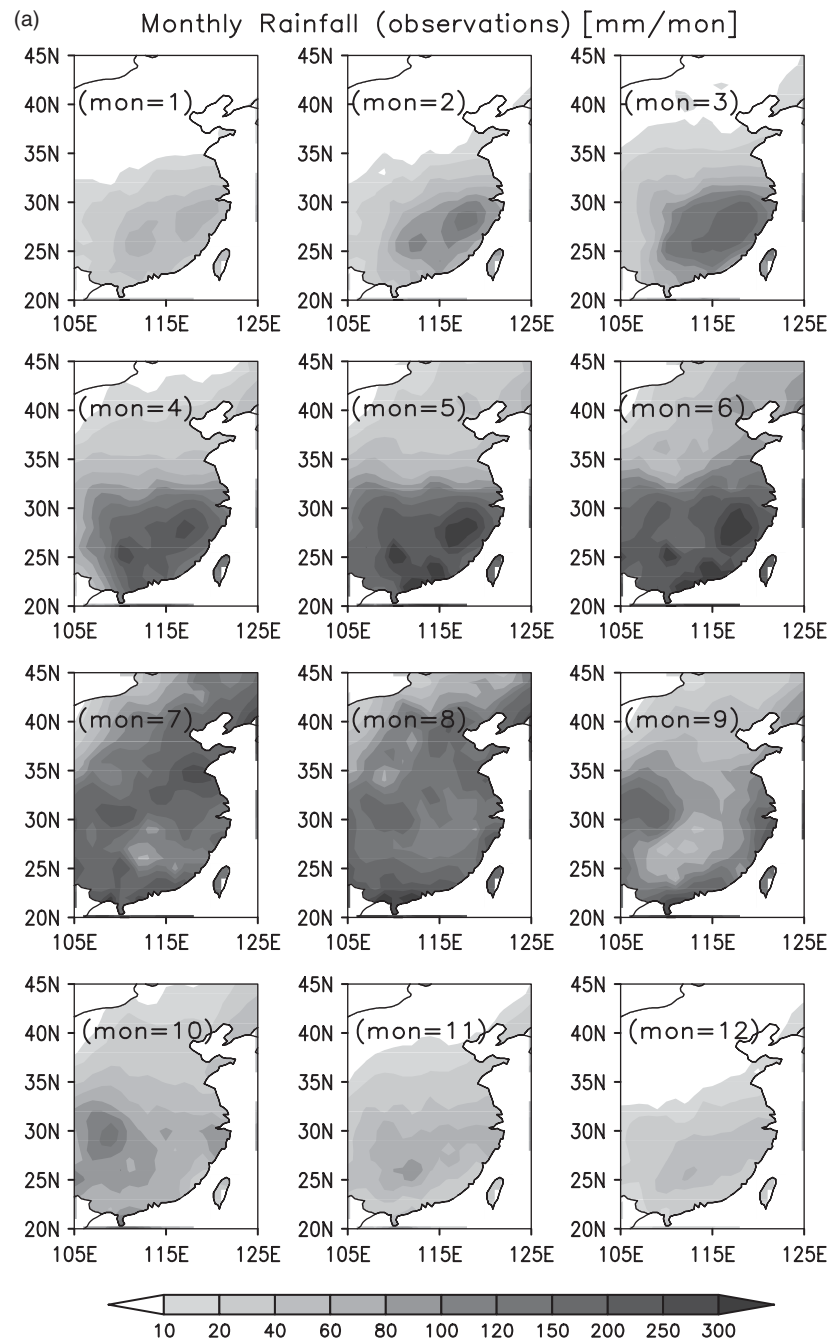


Figure 3. The long-term mean (a) precipitation and (b) runoff depth for each month averaged from 1951 through 1983 over EC. Unit: mm/month.

the Yangtze River and the Nanling Mountain (around 25°N). The runoff depth in this region increases rapidly in these months and peaks in June, with the maximum located around the Wuyi Mountain (25°N to 28°N and 116°E to 121°E) along the southeast coast. The Pearl River Delta (about 23°N and 114°E) on the southern coast is a special region where the runoff does not vary coherently with the precipitation, and it is likely due to the large population and strong human intervention. After the monsoon retreat, when the precipitation intensity reduces substantially, the lag response of runoff is more apparent. In August and September, the large runoff depth belt retreats southward and is mainly located to the south of Nanling Mountain (about 25°N). From

October to December, the main runoff depth belt is located along the lower reaches of the Yangtze River (Figure 3(b)), which is possibly due to the lag response to large precipitation amounts during fall in the upper reaches of its river networks (Figure 3(a)). In general, the runoff depth distribution has more regional characteristics than precipitation but is generally dominated by the amount of precipitation and movement of the precipitation belt.

As shown previously, regional features and north-south movement are important characteristics for the variation of precipitation and runoff. Although, in general, the total amount of both precipitation and runoff depth over the EC peaks in the summer, this is not valid for some

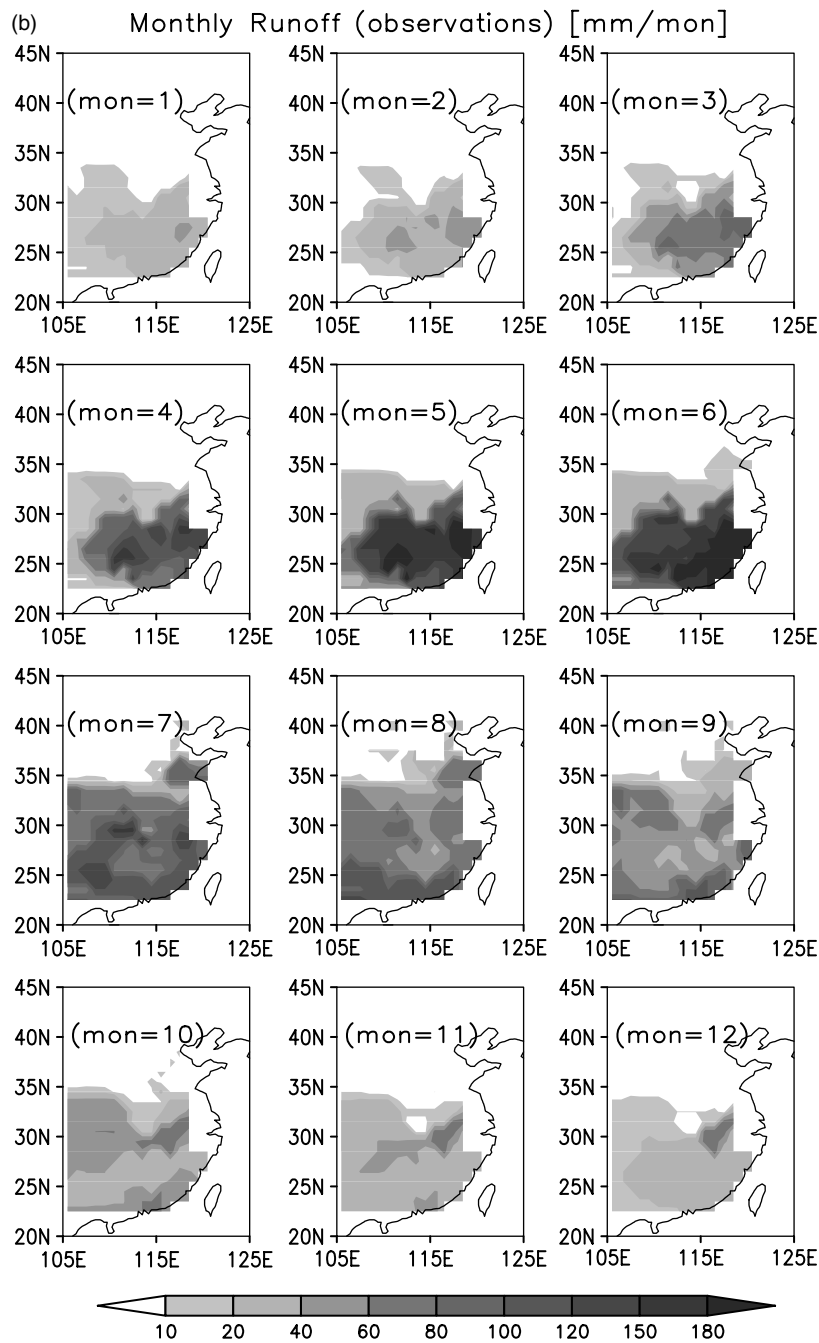


Figure 3. (Continued).

regions. For example, the total precipitation over the EC in spring accounts for 25.6% of the annual amount, which is only about half of that (48.1%) in summer, but it is quite important for large regions in South China, where the precipitation in spring is equal to or even larger than that in summer (Figure 4(a)). A similar relationship exists for the runoff over South China, where the magnitude of runoff in spring is as large as or even 40% larger than that in summer (Figure 4(b)). This indicates that the main characteristic of precipitation/runoff in South China cannot be comprehended if we only consider the situation in summer. So far, the most extensive studies of East Asian climate focus on summer (e.g. Huang and Wu, 1989; Huang and Sun, 1992; Weng *et al.*, 1999; Wang *et al.*,

2000; Ding, 2004; Xue *et al.*, 2005), with less attention being paid to the spring rainfall/runoff variability. Moreover, no comprehensive analyses have been conducted on the interannual variation of spring runoff in China. Hence, in the following two sections, we will focus on the spring precipitation/runoff variabilities and analyze their relationship with the SST.

4. Spatial and temporal spring precipitation and runoff patterns

To analyze the dominant spatial and temporal patterns of spring (MAM) precipitation and runoff depth, we conducted the EOF analyses on the anomaly precipi-

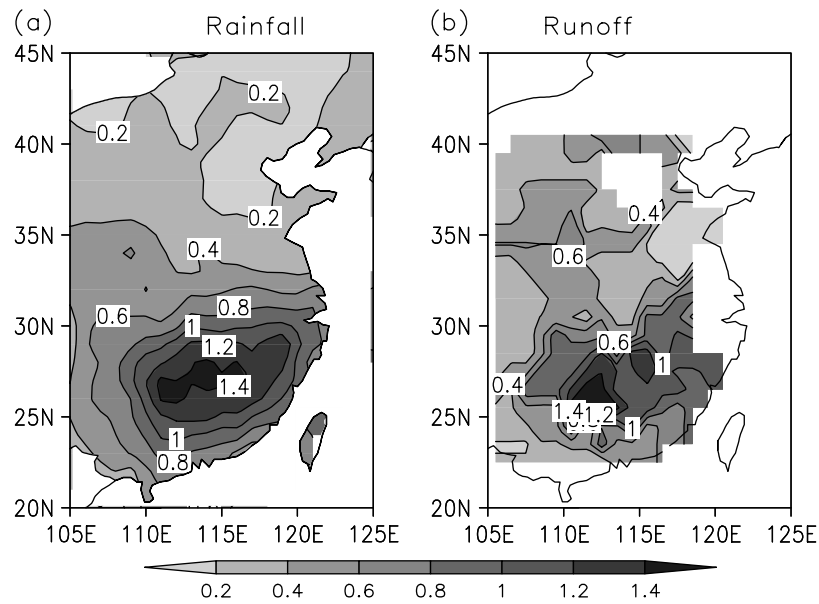


Figure 4. The ratio of long-term mean spring (MAM) to summer (JJA) (a) precipitation and (b) runoff depth for the period 1951–1983.

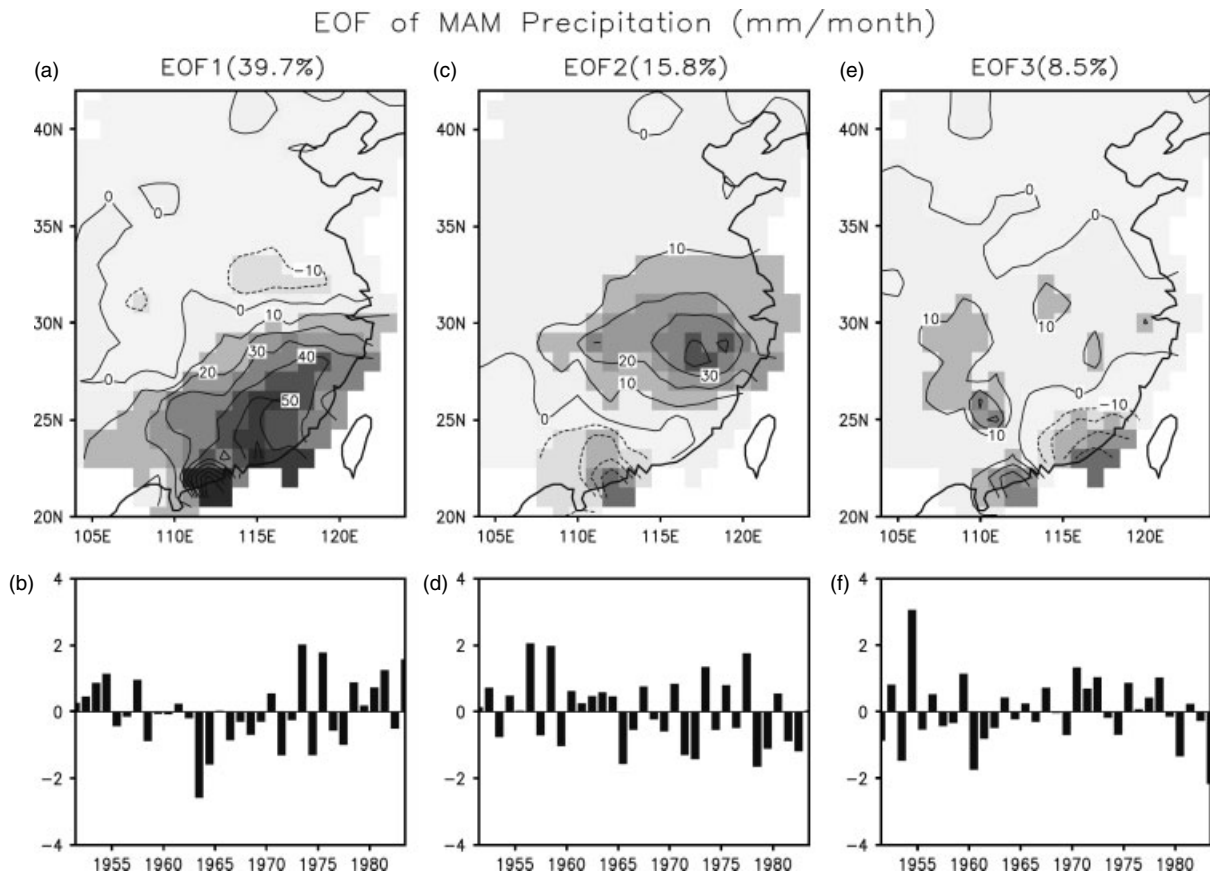


Figure 5. (a) The first EOF mode of spring mean precipitation for the years 1951 through 1983. (b) The normalized principal component (PC) time series for EOF1. (c) and (d), and (e) and (f) are the same as (a) and (b), but for the second and third EOF.

tation/runoff by removing the climatological seasonal cycle, which is defined as the average annual cycle for the data period. In the temporal domain, each PC from EOF analyses is scaled by its standard deviation. The spatial pattern is then multiplied by its corresponding PC's standard deviation.

Figure 5 presents the spatial patterns and their corresponding PCs for the first three EOF modes of the spring precipitation. The first EOF (Figure 5(a)) is similar to that shown by Wu and Kirtman (2007), but with a higher variance (Wu and Kirtman presented only EOF1 of spring rainfall). EOF1_p explains 39.7% of the total variance of

spring rainfall and is well separated from the rest modes according to the criteria of North *et al.* (1982). In this article, we use the suffixes *p* and *r* to denote the precipitation and runoff EOFs, respectively. EOF1_{*p*} is characterized by a dominant positive centre located over South China (Figure 5(a)), which is almost identical to the maximum spring precipitation centre (not shown). In addition, the variation of precipitation in South China is opposite to that in North China, roughly divided by the Yangtze River and with a larger magnitude, suggesting that the dominant mode of spring precipitation in EC represents the intensity of precipitation in South China. PC1_{*p*} is negative most of the time during 1958–72 and mainly positive during the early 1950s and late 1970s (Figure 5(b)). This result implies a decadal variability of spring precipitation intensity and is consistent with Wu and Kirtman (2007).

EOF2_{*p*} explains 15.8% of the total variance and exhibits a north–south oscillation in the EC, mainly to the south of Huaihe River (around 33°N), with the Nanling Mountain (around 25°N) as the boundary dividing the major positive and negative patterns (Figure 5(c)). The major positive anomalies are located in the lower reaches of the Yangtze River with the maximum around the Poyang Lake (29°N and 117°E), and the major negative anomalies are in the Pearl River Delta, on the south slope of Nanling Mountain. These anomalies imply that this mode of precipitation is possibly related to the distribution of topography. The corresponding time series

(Figure 5(d)) shows clear interannual variation with a weak decadal component. EOF3_{*p*} explains only 8.5% of the total variance and represents a roughly south-east–northwest gradient, that is, opposition between the coastal Wuyi Mountain and the area between the south of Qinling Mountain and the Huaihe River (Figure 5(e)). Because the sampling error for EOF3_{*p*}'s eigenvalue [based on North *et al.* (1982)] is larger than the spacing between EOF3_{*p*} and EOF4_{*p*}'s eigenvalues, EOF3_{*p*} has large uncertainty. Nevertheless, we believe that this mode shows an important physical characteristic of spring precipitation in the EC (see discussions in the following third paragraph), so we retain this figure here.

Using the runoff data from 1951 to 1983, three spring runoff EOFs and PCs are shown in Figure 6. As expected, the information is mainly concentrated south of the Yangtze River. EOF1_{*r*} explains 55% of the spring runoff variance in the EC and is well separated from the rest modes according to the criteria of North *et al.* (1982). Similar to the first EOF for precipitation, this pattern is almost identical to the distribution of spring runoff depth in the EC (not shown) and describes the variation of spring runoff intensity in South China. The positive anomalies cover large areas to the south of the Yangtze River, with the maximum positive anomalies being located around the Wuyi Mountain and east of Nanling Mountain (Figure 6(a)), which strongly resembles EOF1_{*p*} (Figure 5(a)). The temporal variations of PC1_{*r*}

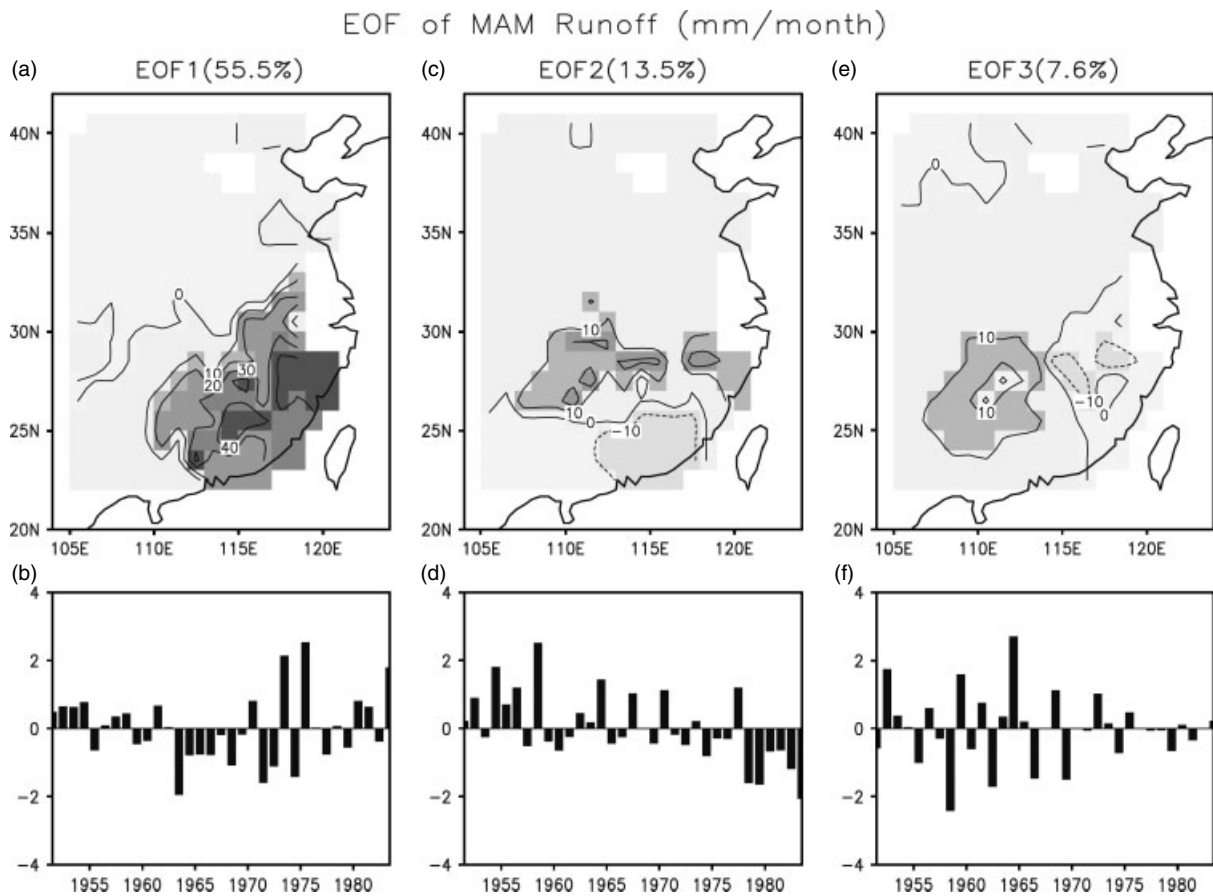


Figure 6. The same as in Figure 5, but for the spring mean runoff depth.

(Figure 6(b)) are also similar to $PC1_p$ (Figure 5(b)), with the correlation coefficient 0.94 far exceeding the 99% confidence level. This result suggests that the leading mode of spring runoff in EC is controlled directly and dominantly by that of spring precipitation.

$EOF2_r$ explains 13.5% of the total variance and exhibits a north–south oscillation in the EC (Figure 6(c)). The positive centres are mainly along the Xiangjiang River Valley and the Ganjiang River Valley, both of which originate north of Nanling Mountain while the relative weak negative centre is located southeast of Nanling Mountain. This pattern is also similar to $EOF2_p$ (Figure 5(c)), indicating a direct response of runoff to precipitation. The corresponding time series shows a strong interannual variation with a declining trend (Figure 6(d)) and is correlated with $PC2_p$, with correlation coefficient 0.83 far exceeding 99% confidence level.

$EOF3_r$ explains only 7.6% of the total variance and represents a clear east–west gradient, with the Luoxiao Mountain as a boundary (Figure 6(e)). This mode has large uncertainty according to the criteria of North *et al.* (1982). However, it resembles $EOF3_p$ to a great extent (Figure 5(e)), with the correlation coefficient between $PC3_r$ and $PC3_p$ 0.71 beyond 99% confidence level. Since the runoff and precipitation data are measured and recorded by two independent organizations, this result implies that the great similarity between $EOF3_r$ and $EOF3_p$ is not by chance. Instead, both of them represent important physical characteristics of spring runoff depth and precipitation in the EC.

In summary, the analyses from these modes suggest that the variabilities of spring runoff have a direct and immediate response to those of the simultaneous *in situ* precipitation. This is an important characteristic of spring runoff and is very different from that in summer (Xue *et al.*, 2005). In addition, the variations of these modes have distinct features. $PC1_r$ is characterized by a dry trend before the middle of the 1970s and by a larger interannual variability after that. $PC2_r$ has a negative trend during the time period. $PC3_r$ is somewhat in contrast to $PC1_r$, with a large interannual variability before 1975 and a smaller one after that. In the following section, we will discuss further the relationship between spring runoff and precipitation and SST, with more emphasis on interdecadal timescales.

5. Correlations between spring runoff, precipitation, and SST

5.1. Interannual timescales

Previous studies (e.g. Huang and Wu, 1989; Chen, 2002) have shown that the East Asian winter and summer monsoon cycle is strongly influenced by ENSO, and the corresponding precipitation pattern further depends on the different phases of the ENSO cycle (Chen, 2002). Since spring is the transitional season between winter and summer, the spring precipitation (and therefore runoff) is also possibly influenced by ENSO (Zhang *et al.*, 1999;

Wang *et al.*, 2000; Wu *et al.*, 2003). In this section, we will first examine the relationship between spring precipitation/runoff depth and ENSO on the interannual timescales.

The multivariate ENSO index ((MEI), Wolter and Timlin, 1993, 1998) is employed to represent the variations of ENSO. It is calculated every month from an analysis of SSTs and air temperatures and other meteorological variables recorded over the tropical Pacific region. In this study, the MEI time series is computed on a bimonthly time scale and downloaded from <http://www.cdc.noaa.gov/ENSO>.

Figure 7 shows the correlation coefficients between 12 MEIs, 3 spring runoff depth PCs, and 3 spring precipitation PCs. It is clear that $PC1_r$ and $PC1_p$ are both significantly related to the MEI of preceding months (Figure 7(a)). Actually, this positive correlation can be traced back to the preceding summer (Figure 8(a)). This good relationship vanishes from the following May/June through August/September. In the succeeding late autumn and winter, the MEI is closely related with $PC1_r$ again with negative correlation, but not with $PC1_p$ (Figure 7(a)). This result indicates that the ENSO's influence on the spring rainfall and runoff in southern China strongly depends on the phase of ENSO with an opposite relationship between the decaying and developing phases, which is consistent with previous precipitation studies (e.g. Wu and Kirtman, 2007).

To confirm this relationship, we further present the regression/correlation map of spring precipitation/runoff depth on the preceding January/February MEI and the following January/February MEI, respectively (Figure 9). When the MEI leads the precipitation/runoff depth, it indicates an influence from the decaying phase of ENSO. During this phase, the spring runoff depth shown in Figure 9(a) presents positive anomalies in southeast China, the pattern of which resembles closely to that in $EOF1_r$ (Figure 6(a)). The precipitation depicts similar anomalies with runoff, but with weaker signals (Figure 9(b)). During the developing phase of ENSO, the MEI lags the precipitation/runoff depth, which indicates that the main EOF mode emerges before the mature phase of ENSO. Both the runoff depth (Figure 9(c)) and the precipitation (Figure 9(d)) present almost the reverse situations to those in the decaying phase of ENSO. This kind of succeeding relationship with MEI has been reported for other land-surface hydrological variables, such as soil moisture (e.g. Yang *et al.*, 1996), but the dynamic and physical implications of this type of relationship are still not well understood.

$PC2_r$ is closely related to the simultaneous and succeeding MEI (Figure 7(b)) but has no significant relationship with the preceding MEI. This indicates $PC2_r$ is not influenced by ENSO, since the oceanic influence can only be established with their covariability when the ocean is leading (Frankignoul and Hasselmann, 1977). The relationship of the north–south oscillation of South China's spring precipitation/runoff with SST will be discussed further in the next session. $PC3_p$ is closely related to MEI

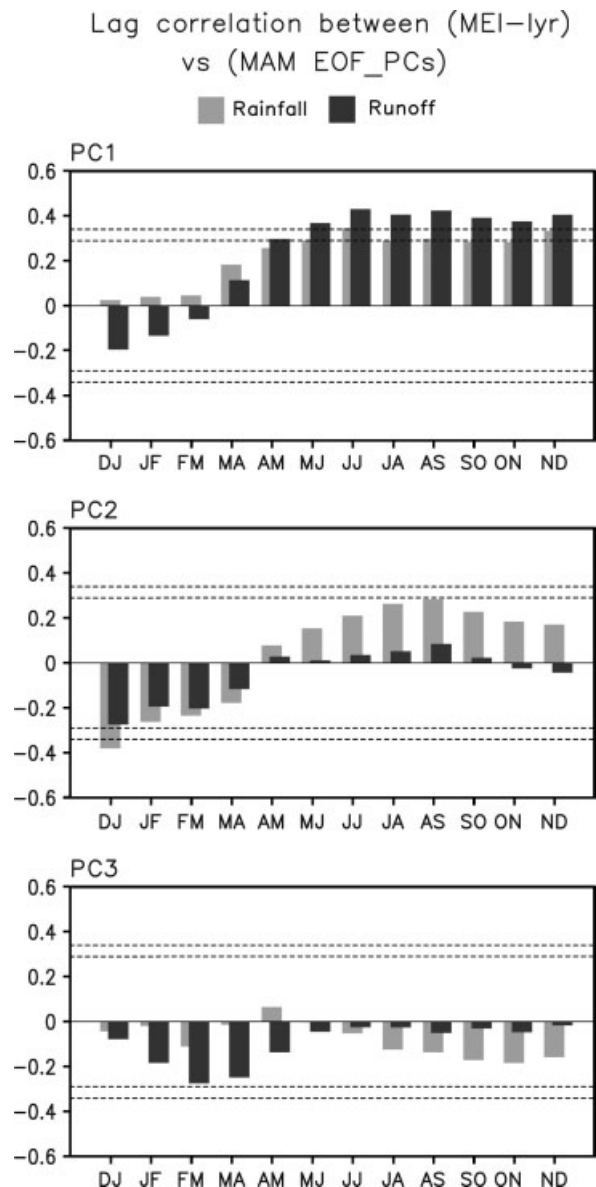
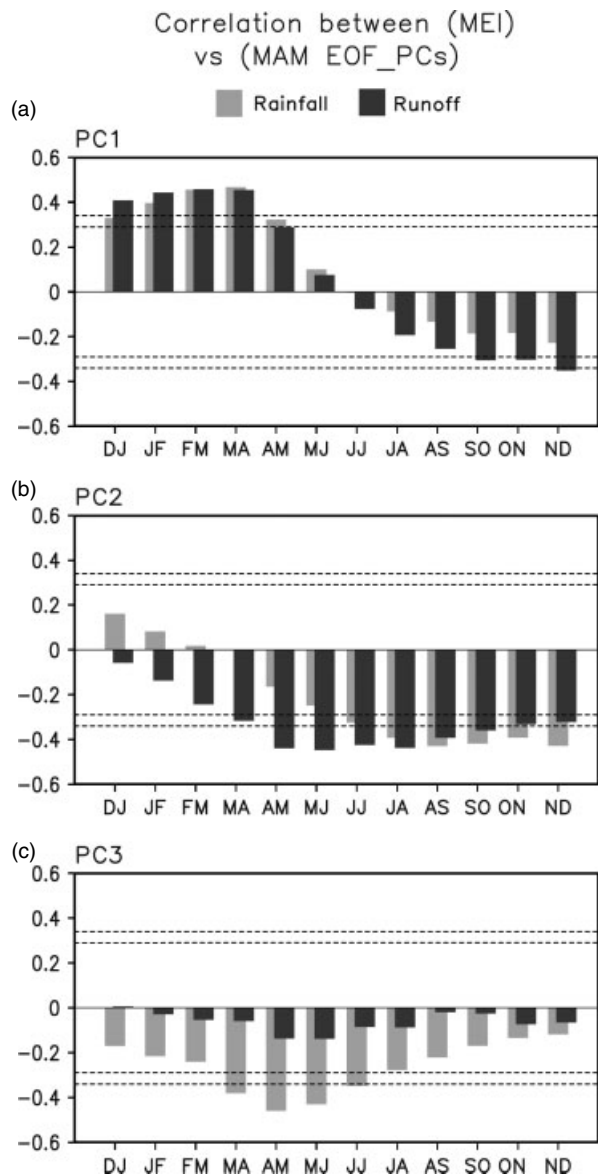


Figure 7. Correlation coefficients between MEI and (a) PC1, (b) PC2, and (c) PC3 of spring (MAM) runoff depth and precipitation. Light bar indicates precipitation and dark bar the runoff. The dashed lines indicate 90% and 95% confidence level.

Figure 8. The same as in Figure 7, but for the MEI of the previous year.

from March to April through the succeeding June–July, after which time the relationship is insignificant. PC3_r is barely related to MEI (Figure 7(c)). There are no significant correlations between MEIs in preceding summer and PC2/PC3 (Figure 8(b) and (c)).

5.2. Interdecadal timescales

As discussed in Section 4, the variations of three dominant modes of precipitation/runoff depth have distinct interdecadal characteristics. In this section, we will further study the relationship between MAM SST and MAM precipitation/runoff on interdecadal timescales through SVD analysis. To extract the decadal components, SST, precipitation, and runoff depth are filtered using a recursive low-pass filter (Kaylor, 1977) to exclude the oscillations with less than 8-year cycles. The data anomalies have been normalized by their standard deviations

first, and then SVD analyses on SST/precipitation and SST/runoff covariability are conducted. In this study, we focus on spatial patterns and time variability rather than absolute amounts. The first two SVD modes for precipitation and runoff will be discussed and compared. We use the suffix *s* to denote the SST anomaly fields.

Figure 10 illustrates the first two pairs of SVD modes between precipitation and SST and the corresponding time series. SVD1 explains 43.2% of the squared covariance. The spatial pattern of SST exhibits an El Niño-like structure, with the strongest signals located in the tropical regions. The warm signals cover large areas in the tropical eastern Pacific, part of the western Pacific, and most of the Indian Ocean, while two cold pools are located in the extratropical Pacific in both the hemispheres (Figure 10(a)). This pattern seems to be more connected with the ENSO-like interdecadal SST signal

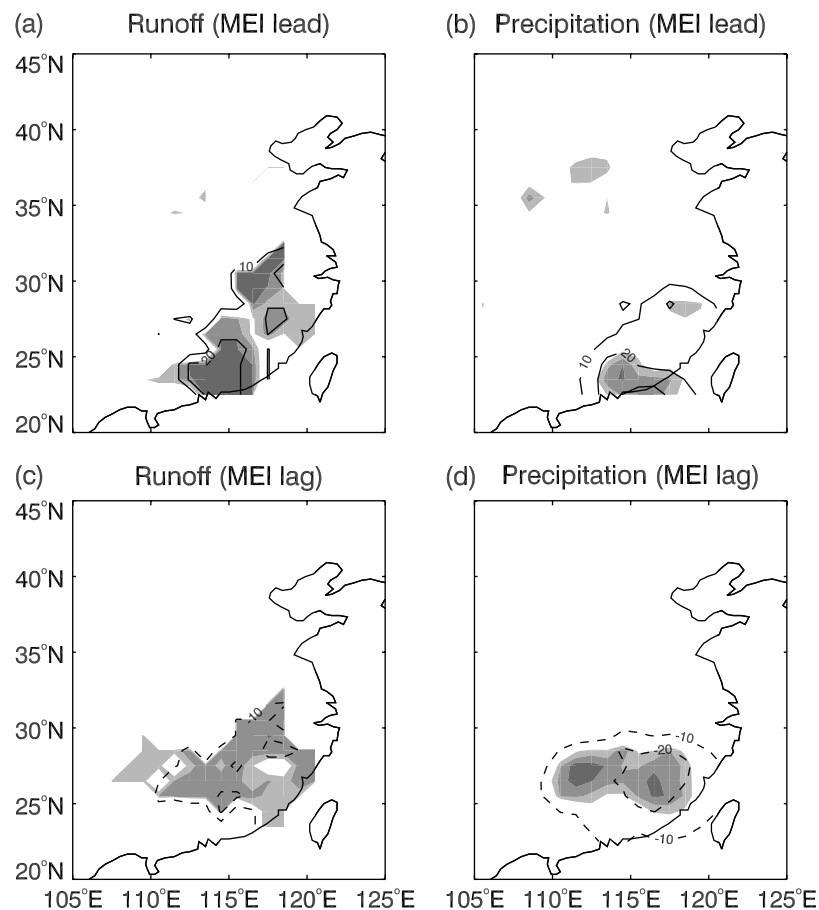


Figure 9. The regression (contour)/correlation (shading) map of spring (MAM) mean (a) runoff depth and (b) precipitation on the normalized MEI of the preceding January/February for the period 1951–1983. Contour intervals are 10 mm/month. Light, middle, and dark shadings indicate 90%, 95%, and 99% confidence level.

(Zhang *et al.*, 1997). The correlations are very high for the tropical eastern Pacific and eastern North Pacific, with absolute correlation coefficients larger than 0.8. SVD1_p is characterized by a distinct meridional positive–negative–positive pattern, with the strongest signal in southeast China (Figure 10(b)). The corresponding time series PC1_s and PC1_p are highly correlated ($r = 0.94$) and exhibit pronounced interdecadal variations with an upward trend after 1976 (Figure 10(c)). This is consistent with previous studies that suggest a warming trend in the tropical eastern Pacific (Mantua *et al.*, 1997; Zhang *et al.*, 1997) and a springtime wetter trend in North and South China (Zhou and Huang, 2006a,b) after the middle of the 1970s, whereas the trend is opposite to the summer precipitation (e.g. Huang *et al.*, 1999, 2003; Zhou and Huang, 2003; Xue *et al.*, 2005).

The fraction of the squared covariance explained by SVD2 of precipitation and SST is 25.3%, with the correlation coefficient between PC2_s and PC2_p being 0.90. In contrast to SVD1, the SST distribution (SVD2_s, Figure 10(d)) presents relatively weaker signals in the tropical areas but stronger signals in extratropical regions. A strong positive signal covers large areas of the Indian Ocean, the Pacific south of 20°S, and the west Pacific. In addition, a negative–positive–negative pattern

appears in the North Pacific. The associated precipitation anomalies exhibit pronounced north–south oscillation with the Yangtze River as a boundary (Figure 10(e)). PC2_s and PC2_p experience roughly one cycle in the 33-year period, with negative phase before 1970 and positive phase after that (Figure 10(f)). SVD2 captures only part of the interdecadal signal left over from SVD1, and the variation of precipitation described by SVD2_p is inconsistent with the dominant observation patterns (Zhou and Huang, 2006a,b); therefore, it is believed that the actual precipitation variance associated with this mode may be very small. Hence, the long-term signal in SST/precipitation is largely contained in SVD1.

The first two pairs of SVD modes between runoff depth and SST and the corresponding time series are presented in Figure 11, with SVD1 explaining 61.2% of the squared variance. The first mode of SST (SVD1_s, Figure 11(a)) has strong signals in the tropical area and eastern North Pacific, resembling the spatial pattern of SVD1_s (Figure 10(a)) but with slightly weaker signals in the tropics. Compared with Figure 10(a), this SVD mode is more like the ENSO-like interdecadal SST signal (Zhang *et al.*, 1997), or namely the *Pacific decadal oscillation* (PDO, Mantua *et al.*, 1997). However, the associated runoff mode (Figure 11(b)) is different from

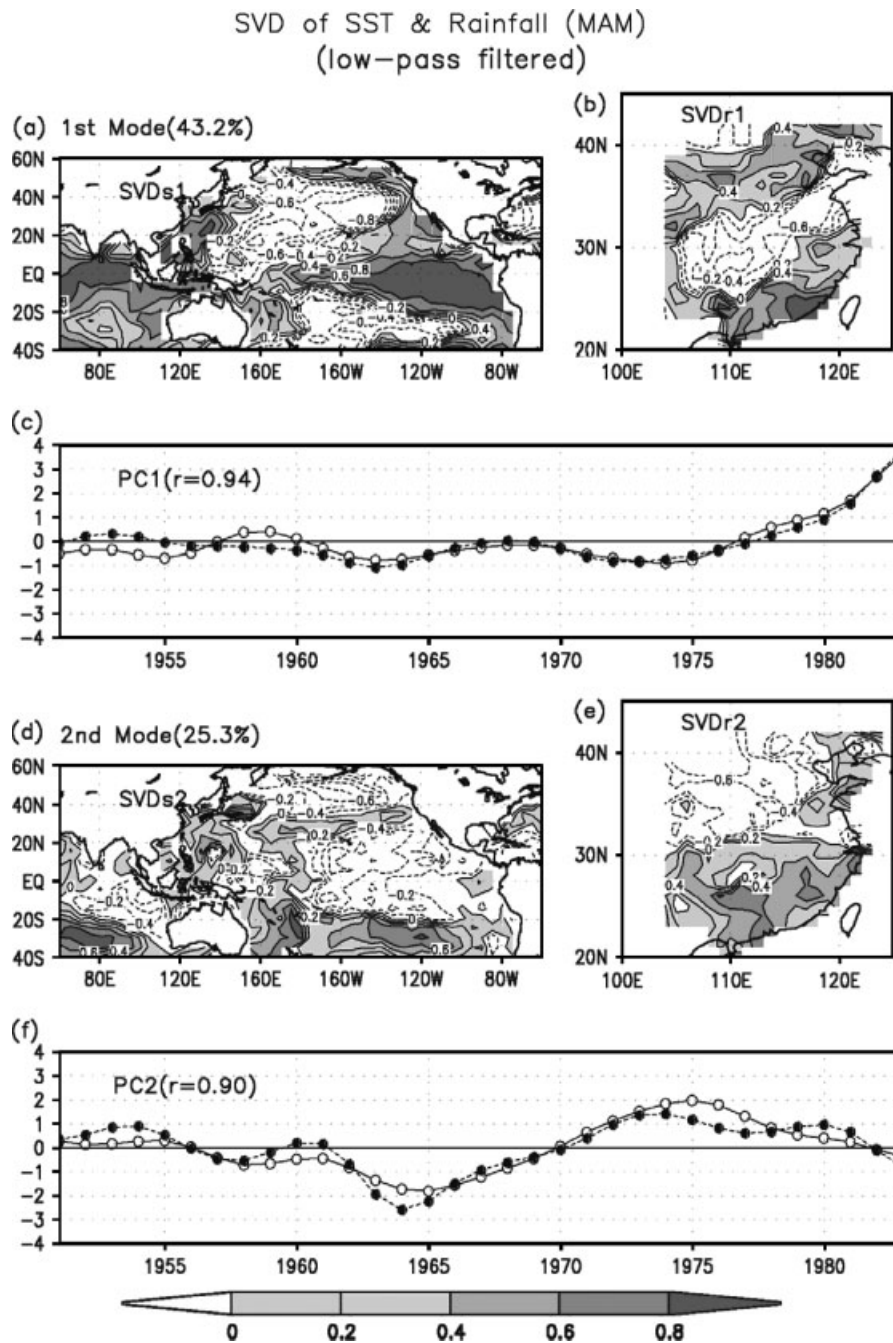


Figure 10. Spring (MAM) SST and precipitation SVD spatial pattern and PC time series during the period 1951–1983. (top) first mode: (a) $SVD1_s$, (b) $SVD1_p$, and (c) $PC1$. (bottom) second mode: (d) $SVD2_s$, (e) $SVD2_p$, and (f) $PC2$. Open and closed circles in (c) and (f) indicate PCs of SST and precipitation, respectively.

that in Figure 10(b) and exhibits a clear north–south gradient in the EC, with the strongest correlation located in the middle and lower reaches of the Yellow River. The corresponding time series $PC1_s$ and $PC1_p$ are highly correlated ($r = 0.92$) and underwent similar interdecadal variations to those in Figure 10(c), with an upward trend after 1965 (Figure 11(c)). This suggests that on the interdecadal timescale, the most dominant change of runoff occurs in North China rather than in southeast China, and it is closely related to the decadal SST variations in the North Pacific. Our result is generally consistent with the studies of Zhou and Huang (2006a,b), which suggest that

the difference between spring precipitation and evaporation in the middle and lower reaches of the Yellow River decreased in the 1960s and increased significantly after the middle of the 1970s.

SVD2 explains 15.6% of the total squared covariance. The $SVD2_s$ pattern (Figure 11(d)) is quite similar to that in Figure 10(d), but with a few differences. The correlation in the Kuroshio and Kuroshi–Oyashio extension regions are not as strong as those in Figure 10(d). In the subtropical south Pacific, the centre of positive correlation moves from about 120°W (Figure 10(d)) to about 140°W (Figure 11(d)), with negative correlation

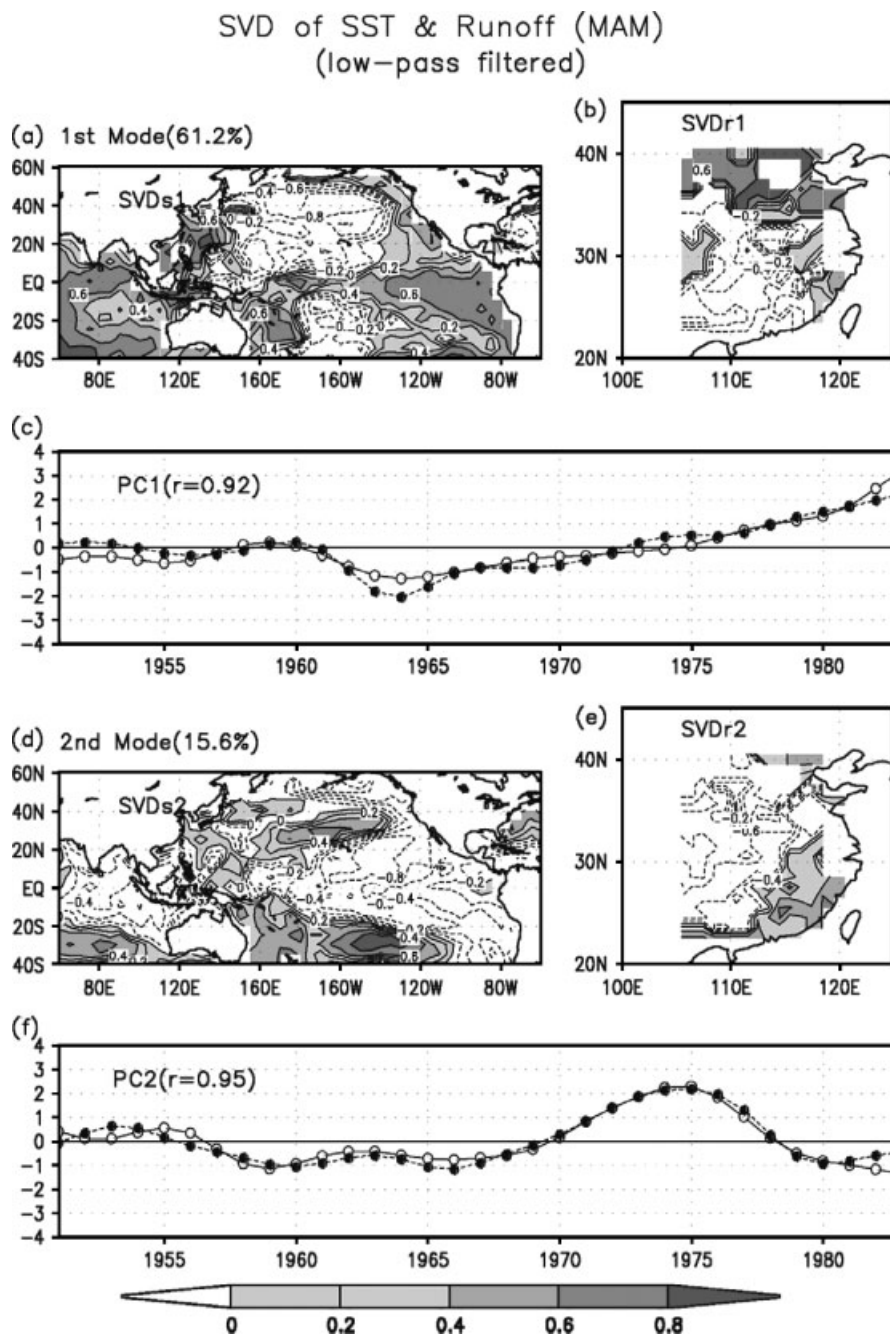


Figure 11. The same as in Figure 8, but for the spring mean runoff depth.

emerging to the east of 100°W (Figure 11(d)). The associated runoff mode (SVD_{2r}, Figure 11(e)) roughly exhibits a northwest–southeast gradient and is different from the north–south pattern in Figure 10(e). The centre of the positive correlation is consistent with the dominant runoff EOF mode. The corresponding time series (Figure 11(f)) has similar interdecadal variations with those in Figure 10(f) for the whole period except after 1975, during which time PC2_s and PC2_p turn to the negative phase rapidly (Figure 11(f)). The second SVD modes of runoff and precipitation in the EC have similar spatial distributions to some extent in general and undergo similar interdecadal variations. The difference of spatial pattern and time

variations between SST/runoff (Figure 11(d)–(f)) and SST/precipitation (Figure 10(d)–(f)) may result mainly from the SST variations in the Kuroshio and Kuroshio–Oyashio extension regions and subtropical south Pacific.

6. Summary

In this study, data from 72 runoff stations and 160 precipitation stations are employed to investigate the annual cycle and variabilities of the spring river runoff in the EC and their relations to precipitation and SST for the period 1951–1983. The climatologically month-to-month evolution of the runoff system in the EC is presented for the first time and compared with that of

precipitation. It is found that the spatial distribution of runoff generally follows that of *in situ* precipitation but has more regional characteristics, which may arise from the effect of topography. The evolution of runoff exhibits a clear north–south movement with time and has diverse peak times for different regions. Since the spring runoff/precipitation accounts for a large portion of the total amount, the interannual variations of runoff and precipitation in spring are the focus of this investigation.

EOF analysis reveals that the leading interannual modes of spring runoff and precipitation illustrate the intensity of runoff and precipitation in South China, which varies in opposite phase to that in North China. These two leading modes are significantly related, suggesting a direct response of runoff to precipitation, in contrast to the summer situation (Xue *et al.*, 2005). Further analysis reveals that the evolution of ENSO event may exert strong influence on these two modes, which is consistent with the previous precipitation studies (e.g. Wu and Kirtman, 2007). The second leading modes of runoff and precipitation are also closely related and illustrate a north–south oscillation in the EC, with the Nanling Mountain (about 25°N) as the boundary. This pattern is mainly determined by the distribution of topography and seems not to be influenced by ENSO. The third leading modes of runoff and precipitation both exhibit similar east–west gradients in EC and are closely related on interannual scales. However, these two modes have some uncertainties; further investigation is necessary for their significance.

On interdecadal timescales, the relationship between spring precipitation/runoff and SST reveals that the leading coupled modes of both precipitation and runoff are closely related to the ENSO-like interdecadal SST signal, which is very strong in the tropical areas (positive signal) as well as in the eastern North Pacific (negative signal). This decadal SST signal has a pronounced upward trend after 1976 and is closely related to the wetter trend in North China after the mid-1970s. In contrast, the SST signal associated with the second leading coupled mode of both precipitation and runoff is weak in the tropical areas and strong in the extratropical oceans, especially in the subtropical South Pacific and the south Indian Ocean. This SST pattern corresponds to the north–south gradient of precipitation/runoff. However, the second coupled mode of precipitation does not resemble the dominant observational facts (Zhou and Huang, 2006a,b). It is believed that the long-term signals in precipitation variance are largely contained in the first coupled mode. In contrast, the second coupled mode of runoff is consistent with the dominant EOF mode of the runoff but explains relatively low variances.

Providing seasonal forecasts of rainfall and/or streamflow is an important challenge in hydrology, with potential benefits in reservoir management, operation of irrigation networks, and flood control, among others. These forecasts can be particularly pertinent for regions that experience significant interannual variability that result from the ENSO phenomenon, as it is often possible to use

the knowledge of ENSO and related oceanic patterns to provide estimates of future rainfall and/or streamflow that outperform the climatological means (Westra *et al.*, 2008). Hence, future work may be done with the extension of our results to characterize the trend quantitatively by using numerical models such as neural network models (Makkeasorn *et al.*, 2008). Further prediction of the streamflow rate may also be made with respect to the findings in this study and be available for use by agriculture, municipal and other sectors.

Acknowledgements

This work is supported by the Chinese Key Developing Program for Basic Sciences (Grant 2004CB418303), the National Natural Science Foundation of China (Grant 40775035), and the US National Science Foundation (Grant NSF-ATM-0353606).

References

- Bretherton CS, Smith C, Wallace JM. 1992. An intercomparison of methods for finding coupled patterns in climate data. *Journal of Climate* **5**: 541–560.
- Chen W. 2002. The impacts of El Niño and La Niña on the cycle of East Asian winter and summer monsoon. *Chinese Journal of Atmospheric Sciences* **26**: 595–610.
- Chen LX, Zhu W, Zhou X. 1998. Studies on climate change in China in recent 45 years. *Acta Meteorologica Sinica* **12**: 1–17.
- Ding YH. 2004. Seasonal march of the East-Asian summer monsoon. In *East Asian Monsoon*, Chang C-P (ed.). World Scientific Publishing Co. Pet. Ltd.: Singapore; 3–53.
- Dirmeyer PA, Dolman AJ, Sato N. 1999. The pilot phase of the global soil wetness project. *Bulletin of the American Meteorological Society* **80**: 851–878.
- Fekete BM, Vorosmarty CJ, Grabs W. 2002. High-resolution fields of global runoff combining observed river discharge and simulated water balances. *Global Biogeochemical Cycles* **16**(3): 1042, 10.1029/1999GB001254.
- Frankignoul C, Hasselmann K. 1977. Stochastic climate models. Part II: Application to sea-surface temperature variability and thermocline variability. *Tellus* **29**: 289–305.
- Huang RH, Sun F. 1992. Impacts of the tropical western Pacific on the East Asian summer monsoon. *Journal of the Meteorological Society of Japan* **70**: 243–256.
- Huang RH, Sun F. 1994. Impact of the thermal state and convective activities over the western Pacific warm pool on summer climate anomalies in East Asia. *Chinese Journal of Atmospheric Sciences* **18**: 262–272.
- Huang RH, Wu Y. 1989. The influence of ENSO on the summer climate change in China and its mechanism. *Advances in Atmospheric Sciences* **6**: 21–32.
- Huang RH, Xu YH, Zhou LT. 1999. The interdecadal variation of summer precipitation in China and the drought trend in North China. *Plateau Meteorology* **18**: 465–475.
- Huang RH, Zhou LT, Chen W. 2003. The progresses of recent studies on the variabilities of the East Asian monsoon and their causes. *Advances in Atmospheric Sciences* **20**: 55–69.
- Kaylor RE. 1977. Filtering and decimation of digital timer series. Technical Report BN 850, Institute of Physical Science and Technology, University of Maryland: College Park, 14.
- Lau KM. 1992. East Asian summer monsoon rainfall variability and climate teleconnection. *Journal of the Meteorological Society of Japan* **70**: 211–242.
- Lau KM, Weng H. 2001. Coherent modes of global SST and summer rainfall over China: An assessment of the regional impacts of the 1997–98 El Niño. *Journal of Climate* **14**: 1294–1308.
- Lau KM, Yang GJ, Shen SH. 1988. Seasonal and intraseasonal climatology of summer monsoon rainfall over East Asia. *Monthly Weather Review* **116**: 18–37.

- Lettenmaier DP, Wood EF, Wallis JR. 1994. Hydro-climatological trends in the continental United States: 1948–88. *Journal of Climate* **7**: 586–607.
- Li H, Robock A, Liu S, Mo X, Viterbo P. 2005. Evaluation of reanalysis soil moisture simulations using updated Chinese soil moisture observations. *Journal of Hydrometeorology* **6**: 180–193.
- Lins HF. 1985. Streamflow variability in the United States: 1931–78. *Journal of Applied Meteorology* **24**: 463–471.
- Makkeasorn A, Chang NB, Zhou X. 2008. Short-term streamflow forecasting with global climate change implications – A comparative study between genetic programming and neural network models. *Journal of Hydrology* **352**: 336–354.
- Mantua NJ, Hare SR, Zhang Y, Wallace JM, Francis RC. 1997. A Pacific interdecadal climate oscillation with impacts on salmon production. *Bulletin of the American Meteorological Society* **78**: 1069–1079.
- Maurer EP, Wood AW, Adam JC, Lettenmaier DP, Nijssen B. 2002. A long-term hydrologically based dataset of land surface fluxes and states for the conterminous United States. *Journal of Climate* **15**: 3237–3251.
- Nitta T, Hu ZZ. 1996. Summer climate variability in China and its association with 500 hPa height and tropical convection. *Journal of the Meteorological Society of Japan* **74**: 425–445.
- North GR. 1984. Empirical orthogonal functions and normal modes. *Journal of the Atmospheric Sciences* **41**: 879–887.
- North GR, Bell TL, Cahalan RF, Moeng FJ. 1982. Sampling errors in the estimation of empirical orthogonal functions. *Monthly Weather Review* **110**: 699–706.
- Oki T, Sud YC. 1998. Design of Total Runoff Integrating Pathways (TRIP) – A global river channel network. *Earth Interactions* **2**: 1–37.
- Parker DE, Rayner NA, Horton EB, Folland CK. 1999. Development of the Hadley Centre sea ice and sea surface temperature data sets (HadSST). *WMO Workshop on Advances in Marine Climatology-CLIMAR99*. Canada, Environment Canada: Vancouver; 194–203.
- Storch HV, Zwiers FW. 1999. *Statistical Analysis in Climate Research*. Cambridge University Press: Cambridge; 484.
- Wallace JM, Smith C, Bretherton CS. 1992. Singular value decomposition of wintertime sea surface temperature and 500-mb height anomalies. *Journal of Climate* **5**: 561–576.
- Wang B, Wu R, Fu X. 2000. Pacific–East Asian teleconnection: How does ENSO affect East Asian climate? *Journal of Climate* **13**: 1517–1536.
- Weng HY, Lau KM, Xue YK. 1999. Long term variations of summer rainfall over China and its possible link to global sea-surface temperature variability. *Journal of the Meteorological Society of Japan* **77**: 845–857.
- Westra S, Sharma A, Brown C, Lall U. 2008. Multivariate streamflow forecasting using independent component analysis. *Water Resources Research* **44**: W02437, DOI:10.1029/2007WR006104.
- Wolter K, Timlin MS. 1993. Monitoring ENSO in LOADS with a seasonally adjusted principal component index. In *Proceedings 17th Climate Diagnostics Workshop*, Norman, NOAA, 52–57.
- Wolter K, Timlin MS. 1998. Measuring the strength of ENSO events: How does 1997/98 rank? *Weather* **53**: 315–324.
- Wu R, Hu ZZ, Kirtman BP. 2003. Evolution of ENSO-related rainfall anomalies in East Asia. *Journal of Climate* **16**: 3742–3758.
- Wu R, Kirtman BP. 2007. Observed relationship of spring and summer East Asian rainfall with winter and spring Eurasian snow. *Journal of Climate* **20**: 1285–1304.
- Xue Y. 1996. The impact of desertification in the Mongolian and the Inner Mongolian grassland on the regional climate. *Journal of Climate* **9**: 2173–2189.
- Xue Y, Sun S, Lau KM, Ji J, Pocard I, Zhang R, Kang HS, Wu G, Schaake JC, Zhang JY, Jiao YJ. 2005. Multi-scale variability of the river runoff system in China and its long-term link to precipitation and sea surface temperature. *Journal of Hydrometeorology* **6**: 550–570.
- Yang S, Lau KM, Sankar-Rao M. 1996. Precursory signals associated with the interannual variability of the Asian summer monsoon. *Journal of Climate* **9**: 949–964.
- Yatagai A, Yasunari T. 1994. Trends and decadal-scale fluctuations of surface air temperature and precipitation over China and Mongolia during the recent 40 year period (1951–1990). *Journal of the Meteorological Society of Japan* **72**: 937–957.
- Zhang R, Sumi A, Kimoto M. 1996. Impact of El Niño on the East Asian monsoon: A diagnostic study of the 86/87 and 91/92 events. *Journal of the Meteorological Society of Japan* **74**: 49–62.
- Zhang R, Sumi A, Kimoto M. 1999. A diagnostic study of the impact of El Niño on the precipitation in China. *Advances in Atmospheric Sciences* **16**: 229–241.
- Zhang Y, Wallace JM, Battisti DS. 1997. ENSO-like interdecadal variability: 1900–1993. *Journal of Climate* **10**: 1004–1020.
- Zhou LT, Huang RH. 2003. Research on the characteristics of interdecadal variability of summer climate in China and its possible cause. *Climatic and Environmental Research* **20**: 55–69.
- Zhou LT, Huang RH. 2006a. Characteristics of interdecadal variability of spring precipitation in North China and its possible cause. *Climatic and Environmental Research* **11**: 441–450.
- Zhou LT, Huang RH. 2006b. Characteristics of temporal and spatial variation of precipitation, evaporation and difference between precipitation and evaporation in North China. *Climatic and Environmental Research* **11**: 280–295.
- Zhuo G, Xie JN, Ma JX. 2000. Statistical relations between typhoon activity and precipitation in China. *Plateau Meteorology* **19**: 260–264.